

# Renormalized spin wave excitations in the antiferromagnetic Heisenberg-Kondo model for heavy fermions

M. Acquarone<sup>1</sup> and C. I. Ventura<sup>2</sup>

<sup>1</sup>*IMEM-CNR and Dipartimento di Fisica, Università di Parma, 43100 Parma, Italy, and*

<sup>2</sup>*Centro Atómico Bariloche, 8400 - Bariloche, Argentina ,*

(Dated: November 25, 2021)

Recent inelastic neutron scattering experiments in CeIn<sub>3</sub> and CePd<sub>2</sub>Si<sub>2</sub> single crystals, measured spin wave excitations at low temperatures. These two heavy fermion compounds exhibit antiferromagnetic long-range order, but a strong competition between the Ruderman-Kittel-Kasuya-Yosida (RKKY) interaction and Kondo effect is evidenced by their nearly equal Néel and Kondo temperatures. Our aim is to show how magnons such as measured in the antiferromagnetic phase of these Ce compounds, can be described with a microscopic Heisenberg-Kondo model as introduced by J.R.Iglesias, C.Lacroix and B.Coqblin, used before for studies of the non-magnetic phase. The model includes the correlated Ce-4*f* electrons hybridized with the conduction band, and we consider competing RKKY (Heisenberg-like  $J_H$ ) and Kondo ( $J_K$ ) antiferromagnetic couplings. Carrying on a series of unitary transformations, we perturbatively derive a second-order effective Hamiltonian which, projected onto the antiferromagnetic electron ground state, describes the spin wave excitations, renormalized by their interaction with correlated itinerant electrons. We numerically study how the different parameters of the model influence the renormalization of the magnons, yielding useful information for the analysis of inelastic neutron scattering experiments in antiferromagnetic heavy fermion compounds. We also compare our results with available experimental data, finding good agreement with the spin wave measurements in cubic CeIn<sub>3</sub>.

PACS numbers: 71.27.+a,75.30.Ds

## I. INTRODUCTION

The description of heavy fermion compounds is challenging due to the rich variety of phase diagrams they present, and the anomalous physical properties which may be found. Among them, appear the Ce and U compounds which exhibit long-range antiferromagnetism (AF) at low temperatures (for example, among antiferromagnetic Ce compounds, CeRh<sub>2</sub>Si<sub>2</sub> exhibits the highest ordering temperature  $T_N = 36K$ , with local magnetic ordered moments of  $1.34 - 1.42\mu_B$  per Ce, i.e. relatively large, compared to the full Ce<sup>3+</sup> free-ion value:  $2.54\mu_B$ ).<sup>1</sup> Depending on the particular compound,<sup>2</sup> the antiferromagnetism takes different forms (magnitude of the local moments varies widely: e.g.  $0.001\mu_B$  as in CeRu<sub>2</sub>Si<sub>2</sub> or  $0.02\mu_B$  in UPt<sub>3</sub>, to  $1.55\mu_B$  as in UCu<sub>5</sub>; as does the spin configuration: with three-, two- or one-dimensional AF structures observed). Antiferromagnetism may also appear competing or coexisting with superconductivity,<sup>3,4</sup> for which spin fluctuation-mediated pairing mechanisms are explored.<sup>5</sup> Non-Fermi liquid behaviour may appear,<sup>6</sup> and quantum criticality has become a subject of intensive study in these compounds, both experimentally and theoretically.<sup>4,7,8,9,10,11</sup> The crossover from the antiferromagnetic state to the non-magnetic heavy fermion state, which can be tuned by pressure, doping or magnetic field, is one of the most interesting problems in strongly correlated  $f$ -compounds.

The physical properties of these compounds are determined by the strongly correlated  $f$ -electrons present ( $4f$  in Ce;  $5f$  in U) and their hybridization with the conduction band. The RKKY indirect exchange interaction be-

tween  $f$ -local magnetic moments, favouring the establishment of long-range magnetic order, competes with the screening of these moments by the conduction electrons, described by the Kondo effect.<sup>12</sup> This competition is the subject of the Doniach diagram,<sup>13</sup> which compares the variation of the Néel and Kondo-impurity temperatures with increasing antiferromagnetic intrasite exchange coupling  $J_K$ , between local  $f$ -moments and conduction electron spins. Compounds with similar magnetic ordering temperature  $T_N$  and Kondo temperature  $T_K$ , the temperature below which magnetic susceptibility saturates indicating coherent Kondo-singlet formation, are ideally suited to the study of this RKKY-Kondo competition. In this regard, experiments on CeM<sub>2</sub>Sn<sub>2</sub> (M=Ni, Ir, Cu, Rh, Pd, and Pt:  $4d$  or  $5d$  transition metals)<sup>14</sup> and CeX<sub>2</sub>Si<sub>2</sub> (X=Au, Pd, Rh, Ru)<sup>15</sup> were undertaken, indicating that departures between theory and experiments resulted from the use of Kondo impurity relations. The Kondo-lattice model, instead, consisting of a lattice of local magnetic moments coexisting with a conduction band, has proved appropriate for the description of many  $4-f$  and  $5-f$  materials, in particular most Ce (or Yb) compounds, respectively corresponding to a configuration close to  $4f^1$  (or  $4f^{13}$ ), where one  $4f$  electron (or hole) interacts with the conduction electrons.<sup>10,16,17,18</sup> In 1997 a revisited Doniach diagram was introduced, including short-range antiferromagnetic correlations in the Kondo lattice, in order to improve the description and, in particular, to account for the observed pressure dependence of  $T_K$  in CeRh<sub>2</sub>Si<sub>2</sub>.<sup>16</sup> The situation is more complex in Uranium compounds, where U has a  $5f^n$  configuration with  $n=2$  or  $3$ , since the  $5f$  electrons are much less localized than the  $4f$  electrons of rare earths. Regarding

spin dynamics, it is not clear that Ce and U compounds are intrinsically similar.<sup>2</sup> In the following we will focus on Ce-compounds, except otherwise specifically stated.

Experimentally, while the magnetic response due to Kondo spin fluctuations in the paramagnetic state of heavy fermions is well studied, relatively little is known about the nature of the magnetic excitations in the *ordered* phase of Kondo lattices,<sup>2</sup> on which our present study will focus. Being still an unsolved problem how to describe on equal terms both the Kondo effect and antiferromagnetism,<sup>19</sup> here we will focus on systems with relatively large local moments and study them deep inside the antiferromagnetic phase: far from the antiferromagnetic quantum critical point, where spin fluctuations would become more relevant.

A few years ago CePd<sub>2</sub>Si<sub>2</sub><sup>20</sup> single crystals were studied with inelastic neutron scattering: below the antiferromagnetic ordering temperature strongly dispersive spin wave excitations were found, with an anisotropic damping, which coexisted with the Kondo-type spin fluctuations also present above  $T_N$ . At  $T = 1.5K$  these spin waves were measured along various BZ paths: they were found to present an energy gap of 0.83 meV and to extend up to almost 3.5 meV. CePd<sub>2</sub>Si<sub>2</sub> has a bcc tetragonal structure, and its antiferromagnetic ground state is characterized by propagation vector:  $\vec{q} = (1/2, 1/2, 0)$ , with ordered moments:  $m = 0.66\mu_B$ ,  $T_N = 8.5K$  and  $T_K = 10K$ , and linear electronic specific heat coefficient  $\gamma = 250mJ/molK^2$ . Under pressure application, at 28.6 kbar the system undergoes a transition into a superconducting phase with critical temperature of 430 mK.<sup>21,22</sup> More recently, inelastic neutron studies of CeIn<sub>3</sub> single crystals were performed, with similar results.<sup>21</sup> Well defined spin wave excitations with a bandwidth of 2meV and a gap of 1.28 meV were found in the antiferromagnetic phase,<sup>21</sup> coexisting with Kondo-type spin fluctuations and crystal-field excitations which also appeared above  $T_N = 10K = T_K$ . CeIn<sub>3</sub> crystallizes in a cubic (fcc) structure, with an antiferromagnetic structure characterized by magnetic propagation vector  $\vec{q} = (1/2, 1/2, 1/2)$ , with ordered moments:  $m = 0.5\mu_B$  and  $\gamma = 130mJ/molK^2$ . Under application of pressure, at 26.5 kbar the system undergoes a transition into a superconducting phase with critical temperature of 200 mK.<sup>21</sup>

In next section, we will briefly introduce the microscopic Heisenberg-Kondo model proposed by J.R.Iglesias, C.Lacroix and B.Coqblin,<sup>16</sup> to study the non-magnetic phase of heavy fermion AF compounds, to which we shall add conduction electron correlations. We will then present our calculation for the renormalization of spin wave excitations due to their interaction with the correlated conduction electrons (the Appendix complements this section). In Section III, we will discuss the results of our study, show how the different parameters of the model influence the renormalization of the magnons, and compare our results with the available experimental data.<sup>20,21</sup> In Section IV we summarize and point out that

the present work should yield useful information for the analysis and prediction of inelastic neutron scattering experiments in heavy fermion AF compounds, as CeRh<sub>2</sub>Si<sub>2</sub>.

## II. MICROSCOPIC MODEL, AND PERTURBATIVE APPROACH.

In order to describe the Ce-heavy fermion systems exhibiting antiferromagnetic long-range order we have used the microscopic model which has been proposed by Coqblin et al.<sup>16</sup> to describe the competition between the Kondo effect and the RKKY interaction, in compounds where departures from the original Doniach picture<sup>13</sup> appear. In principle, both the RKKY magnetic coupling and the Kondo effect can be obtained from the Kondo intrasite-exchange term, but when dealing with approximations it is difficult to insure that both effects are taken into account if an explicit intersite exchange (as the effective RKKY interaction or, depending on the system, also the direct exchange) is not included in the Hamiltonian.<sup>10</sup> The model<sup>16</sup> consists of a Kondo lattice, featuring local magnetic moments coupled both to conduction electrons, by a Kondo-type interaction  $J_K$ , and among themselves by an antiferromagnetic RKKY-type exchange  $J_H > 0$ . The moments are assumed to order below the Néel temperature  $T_N$ . The Hubbard-correlated conduction electrons occupy a non-degenerate band. Therefore, the model may be represented in standard notation by the following Heisenberg-Kondo Hamiltonian:

$$H = H_{band} + H_{Kondo} + H_{Heis} \quad (1)$$

$$H_{band} = \sum_{l\sigma} \epsilon_l n_{l\sigma} + \sum_{l\langle j\rangle\sigma} t_{lj} c_{l\sigma}^\dagger c_{j\sigma} + U \sum_l n_{l\uparrow} n_{l\downarrow} \quad (2)$$

$$H_{Kondo} = J_K \left( \sum_{l \in \mathcal{A}} \mathbf{s}_l \cdot \mathbf{S}_l + \sum_{j \in \mathcal{B}} \mathbf{s}_j \cdot \mathbf{S}_j \right) \quad (3)$$

$$H_{Heis} = J_H \sum_{l\langle j\rangle} \mathbf{S}_l \cdot \mathbf{S}_j \quad (4)$$

Here  $l\langle j\rangle$  indicates that the lattice site index  $j$  runs over the  $z$  nearest neighbours of site  $l$ . The itinerant electron spin is  $s_l$ , while  $\mathcal{A}, \mathcal{B}$  label the two interpenetrating sublattices of local moments,  $S_{l \in \mathcal{A}}$  and  $S_{j \in \mathcal{B}}$ , with opposite moment direction. The Kondo exchange  $J_K$  could in principle have either sign (though for heavy fermion compounds, it would be antiferromagnetic:  $J_K \geq 0$ ). In the following we shall distinguish in the Kondo term the longitudinal  $H_K^z$  from the transverse  $H_K^\perp$  contributions. By taking as positive  $z$  direction the direction of  $S_{l \in \mathcal{A}}$ , they are defined as:

$$H_K^z = J_K \left( \sum_{l \in \mathcal{A}} s_l^z S_l^z + \sum_{j \in \mathcal{B}} s_j^z S_j^z \right) \quad (5)$$

$$H_K^\perp = \frac{J_K}{2} \left[ \sum_{l \in \mathcal{A}} (s_l^+ S_l^- + H.c.) + \sum_{j \in \mathcal{B}} (s_j^+ S_j^- + H.c.) \right]$$

We diagonalize the Heisenberg term, by representing the local moments operators in the Holstein-Primakoff approximation, which is appropriate at temperatures much lower than  $T_N$ . Namely, we take

$$\begin{aligned}\vec{S}_i &= (S_i^+, S_i^-, S_i^z) \\ &\sim (\sqrt{2S}b_i, \sqrt{2S}b_i^\dagger, S - b_i^\dagger b_i) \\ \vec{S}_j &\sim (\sqrt{2S}b_j^\dagger, \sqrt{2S}b_j, -(S - b_j^\dagger b_j)),\end{aligned}\quad (6)$$

where  $b_i^{(\dagger)}$  and  $b_j^{(\dagger)}$  are the bosonic operators in sublattices  $\mathcal{A}$  and  $\mathcal{B}$ , respectively. Going to reciprocal space in the reduced Brillouin zone (RBZ) and introducing the AF spin wave operators  $\{a_q^\dagger, a_q\}$  by the Bogolyubov transformation:

$$\begin{aligned}a_q^\dagger &= b_q^\dagger \text{Ch}(\vartheta_q) - b_{-q} \text{Sh}(\vartheta_q) \\ a_q &= b_q \text{Ch}(\vartheta_q) - b_{-q}^\dagger \text{Sh}(\vartheta_q)\end{aligned}\quad (7)$$

where :  $\text{Th}(2\vartheta_q) = -\frac{1}{z} \sum_{\Delta_{lj}} \cos(q\Delta_{lj})$  (8)

diagonalizes  $H_{Heis}$ . In the absence of the interaction with the fermions, i.e. in the limit of vanishing  $J_K$ , the frequency of the bare AF spin waves would be ( $z$  is the number of nearest neighbors and  $\Delta_{lj}$  is the vector joining two n.n.sites)

$$\begin{aligned}H_{Heis} &= \sum_q \hbar\omega_q \left( a_q^\dagger a_q + \frac{1}{2} \right) \\ \hbar\omega_q &= zJ_H S \sqrt{1 - \left[ \frac{\sum_{\Delta_{lj}} \cos(q\Delta_{lj})}{z} \right]^2}\end{aligned}\quad (9)$$

We further assume that the band electrons have developed an AF spin order, due to the cooperating effects of the Hubbard correlation  $U$  and of the interactions with the AF-ordered local moments, which provide a staggered field.

To diagonalize  $H_{band}$  in the AF state, we will use a reformulation of Gutzwiller's variational approach for the description of antiferromagnetism in narrow bands due to Spalek et al.<sup>23</sup> This approach allows to connect the standard (mean-field) Slater band-insulator to the localized Mott antiferromagnetic insulator. One expresses the correlation-induced bandwidth reduction in the paramagnetic (PM) state by a Gutzwiller-type factor  $\Phi(n, \eta)$  depending on the band filling  $n$  and on the probability of double occupancy  $\eta = N^{-1} \sum_l \langle n_{l\uparrow} n_{l\downarrow} \rangle$ . The correlated band energies  $\varepsilon_k^U$  are written as  $\varepsilon_k^U = \Phi(n, \eta) \varepsilon_k^0$ , where  $\varepsilon_k^0$  are the uncorrelated band energies and:

$$\Phi(n, \eta) = 1 - \left( \frac{n}{2-n} \right) \left( 1 - \frac{4\eta}{n^2} \right) \quad (10)$$

The  $U$ - depending optimal value of  $\eta$  is found at zero temperature by minimizing the PM energy

$$E^{PM} = \sum_{k\sigma} \Phi(n, \eta) \varepsilon_k^0 \langle n_{k\sigma} \rangle + NU\eta$$

at given  $n$  and  $U$ .

Assuming that the electrons have an AF ground state of Néel-type one adopts the standard Slater formalism, only with the PM energies renormalized according to Eq.10.

We introduce the fermion operators for this AF Slater-type state  $\{\alpha_{k\sigma}^{(\dagger)}, \beta_{k\sigma}^{(\dagger)}\}$  by the transformation

$$\begin{aligned}c_{k\sigma}^\dagger &= \beta_{k\sigma}^\dagger \cos \zeta_{k\sigma} - \alpha_{k\sigma}^\dagger \sin \zeta_{k\sigma} \\ c_{k+\mathcal{Q},\sigma}^\dagger &= \beta_{k\sigma}^\dagger \sin \zeta_{k\sigma} + \alpha_{k\sigma}^\dagger \cos \zeta_{k\sigma}\end{aligned}\quad (11)$$

where  $\mathcal{Q}=(1/2, 1/2, 1/2)$  in units of  $2\pi/a$  is the wavevector characterizing the AF magnetic state and  $k$  is a wavevector belonging to the reduced Brillouin zone (RBZ) defined by  $|\mathbf{k}| \leq |\mathcal{Q}/2|$ . The diagonalization condition for a lattice with an inversion center yields:

$$\tan(2\zeta_{k\sigma}) = -\sigma \frac{U \langle s \rangle}{\Phi \varepsilon_k} \equiv \sigma \tan(2\zeta_k), \quad (12)$$

where the AF order parameter  $\langle s_i^z \rangle \equiv \langle s \rangle$  of the itinerant electrons (staggered magnetization), or band electron polarization, is given by:

$$\langle s \rangle = -\frac{1}{2N} \sum_{k \in RBZ, \sigma} \left( \langle n_{k\sigma}^\alpha \rangle - \langle n_{k\sigma}^\beta \rangle \right) \sin 2\zeta_k$$

Therefore, the diagonal bare electron Hamiltonian reads:

$$H_{band}^{AF} = \sum_{k \in RBZ, \sigma} \left[ E_{k\sigma}^\alpha n_{k\sigma}^\alpha + E_{k\sigma}^\beta n_{k\sigma}^\beta \right] - UN \left( \frac{n^2}{4} - \langle s \rangle^2 \right), \quad (13)$$

where, assuming that the lattice has a center of inversion, the bare electron eigenenergies (actually spin-independent) read ( $x = \alpha, \beta$ ):

$$E_{k\sigma}^x = \frac{1}{2}Un + (1 - 2\delta_{x\alpha}) \sqrt{\Phi^2 \varepsilon_k^2 + (U \langle s \rangle)^2}, \quad (14)$$

where  $\delta_{x\alpha}$  denotes the Kronecker delta. Notice that  $\alpha$  is the lower subband. The subband filling factors  $\langle n_{k\sigma}^x \rangle = \langle n_{k, -\sigma}^x \rangle = [\exp(E_{k\sigma}^x - \mu) / k_B T + 1]^{-1}$  also depend on  $\langle s \rangle$  through  $E_{k\sigma}^x$ .

### A. Renormalization of the bare subsystems by part of $H_K^z$

By expressing the longitudinal Kondo term in terms of the AF bare electron operators  $\{\alpha_{k\sigma}^{(\dagger)}, \beta_{k\sigma}^{(\dagger)}\}$  and the bare bosonic operators  $\{a_q^{(\dagger)}\}$ , it can be rewritten and decomposed into contributions which are respectively diagonal in the bare bosons, i.e.  $H_K^{z(d)}$ , or non-diagonal, i.e.  $I^z$ .

Explicitly, the diagonal term reads:

$$\begin{aligned}H_K^{z(d)} &= -\frac{J_K}{2} S \sum_{k, \sigma} [\sin(2\zeta_k) (n_{k\sigma}^\alpha - n_{k\sigma}^\beta) \\ &\quad - \sigma \cos(2\zeta_k) (\alpha_{k\sigma}^\dagger \beta_{k\sigma} + \beta_{k\sigma}^\dagger \alpha_{k\sigma})] [1 - V_q]\end{aligned}\quad (15)$$

where the bosonic operator  $V_q$  reads:

$$\begin{aligned} V_q &= \frac{1}{NS} \sum_q \left( a_q^\dagger a_q + a_{-q}^\dagger a_{-q} \right) \text{Ch}(2\vartheta_q) \\ &+ \frac{1}{NS} \sum_q \left( a_q^\dagger a_{-q}^\dagger + a_q a_{-q} \right) \text{Sh}(2\vartheta_q) \\ &+ \frac{2}{NS} \sum_q \text{Sh}^2(\vartheta_q) \end{aligned} \quad (16)$$

The term  $I^z$ , non-diagonal in the bare bosons, will be discussed in next section.

Now, we treat  $H_K^{z(d)}$  in mean-field approximation (MFA), obtaining three kinds of terms. The first one, obtained averaging over the bare electrons reads:

$$\begin{aligned} H_K^{z(d1)} &= -J_K \langle s \rangle \sum_q \left( a_q^\dagger a_q + a_{-q}^\dagger a_{-q} \right) \text{Ch}(2\vartheta_q) \quad (17) \\ &- J_K \langle s \rangle \sum_q \left( a_q^\dagger a_{-q}^\dagger + a_q a_{-q} \right) \text{Sh}(2\vartheta_q) + \text{const.} \end{aligned}$$

and renormalizes the spin wave frequencies, therefore modifying the diagonalization condition (Eq. (8)) for the AF Heisenberg Hamiltonian as:

$$\text{Th}(2\vartheta_q) = -\frac{J_H S \sum_{\Delta l_j} \cos(q\Delta l_j)}{z J_H S - J_K \langle s \rangle} \quad (18)$$

Notice that, in order to minimize the mean-energy of the Kondo term,  $-J_K \langle s \rangle$  is a non-negative quantity, irrespective of the sign of  $J_K$ .

The MFA-redefined Heisenberg term now reads:

$$\bar{H}_{Heis} = \sum_q \hbar \Omega_q \left( a_q^\dagger a_q + \frac{1}{2} \right) \quad (19)$$

with the MFA-renormalized frequency given by:

$$\hbar \Omega_q \equiv (z J_H S + |J_K \langle s \rangle|) \sqrt{1 - \left[ \frac{\sum_{\Delta l_j} \cos(q\Delta l_j)}{z + |J_K \langle s \rangle| / J_H S} \right]^2} \quad (20)$$

Averaging over the bare bosons yields two terms. To write them it is convenient to define the local moment reduction factor as follows:

$$\mathcal{N}_{sw} \equiv \frac{2}{N} \sum_q \left[ \langle a_q^\dagger a_q \rangle \text{Ch}(2\vartheta_q) + \text{Sh}^2(\vartheta_q) \right] \quad (21)$$

where the mean number of MFA bosons is  $\langle a_q^\dagger a_q \rangle = [\exp(\hbar \Omega_q / k_B T) - 1]^{-1}$ . Then the (in general temperature-dependent) expectation value of the local moment is  $\langle S^z \rangle = S - \mathcal{N}_{sw}$ .

The second contribution, which reads

$$H_K^{z(d2)} = -\frac{J_K}{2} \langle S^z \rangle \sum_{k,\sigma} \sin(2\zeta_k) \left( n_{k\sigma}^\alpha - n_{k\sigma}^\beta \right) \quad (22)$$

renormalizes the electron eigenenergies. The diagonalization condition for the AF electron Hamiltonian now is:

$$\tan(2\zeta_{k\sigma}) = -\sigma \frac{U \langle s \rangle - J_K \langle S^z \rangle / 2}{\Phi \varepsilon_k} \quad (23)$$

Consequently, the AF order parameter  $\langle s \rangle$  of the itinerant electrons is given by:

$$\langle s \rangle = \frac{1}{2N} \sum_{k\sigma} \frac{[U \langle s \rangle - J_K \langle S^z \rangle / 2] \left( \langle n_{k\sigma}^\alpha \rangle - \langle n_{k\sigma}^\beta \rangle \right)}{\sqrt{\Phi^2 \varepsilon_k^2 + [U \langle s \rangle - J_K \langle S^z \rangle / 2]^2}} \quad (24)$$

and the MFA eigenenergies by ( $x = \alpha, \beta$ ):

$$E_{k\sigma}^x = \frac{1}{2} U n + (1 - 2\delta_{x\alpha}) \sqrt{\Phi^2 \varepsilon_k^2 + [U \langle s \rangle - J_K \langle S^z \rangle / 2]^2} \quad (25)$$

The third contribution  $H_K^{z(d3)}$  provides a hybridization between the  $\alpha, \beta$  electron states

$$H_K^{z(d3)} = \frac{J_K}{2} \langle S^z \rangle \sum_{k\sigma} \sigma \cos(2\zeta_k) \left( \alpha_{k\sigma}^\dagger \beta_{k\sigma} + \beta_{k\sigma}^\dagger \alpha_{k\sigma} \right) \quad (26)$$

The transformation

$$\begin{aligned} \alpha_{k\sigma}^\dagger &= A_{k\sigma}^\dagger \cos \xi_{k\sigma} + B_{k\sigma}^\dagger \sin \xi_{k\sigma} \\ \beta_{k\sigma}^\dagger &= B_{k\sigma}^\dagger \cos \xi_{k\sigma} - A_{k\sigma}^\dagger \sin \xi_{k\sigma} \end{aligned} \quad (27)$$

where:

$$\tan(2\xi_{k\sigma}) = \sigma \frac{-J_K \langle S^z \rangle \cos(2\zeta_k)}{E_k^\alpha - E_k^\beta - J_K \langle S^z \rangle \sin(2\zeta_k)} \quad (28)$$

allows to eliminate  $H_K^{z(d3)}$  yielding the MFA hybridized electron Hamiltonian in diagonal form as:

$$\bar{H}_{band}^{AF} = \sum_{k\sigma} \left[ \mathcal{E}_{k\sigma}^B n_{k\sigma}^B + \mathcal{E}_{k\sigma}^A n_{k\sigma}^A \right] \quad (29)$$

The hybridized band energies are ( $X = A, B$ )

$$\mathcal{E}_k^X = \frac{1}{2} \left( E_k^\alpha + E_k^\beta \right) - (2\delta_{XA} - 1) \frac{\Gamma_k}{2} \quad (30)$$

where

$$\begin{aligned} \Gamma_k &= \left| E_k^\alpha - E_k^\beta \right| \times \\ &\times \sqrt{\left[ 1 - \frac{J_K \langle S^z \rangle \sin(2\zeta_k)}{E_k^\alpha - E_k^\beta} \right]^2 + \left[ \frac{J_K \langle S^z \rangle \cos(2\zeta_k)}{E_k^\alpha - E_k^\beta} \right]^2} \end{aligned} \quad (31)$$

is the difference of energy at wvector  $k$  between the AF subbands. Notice that the  $A$  band is the lower one. Taking the paramagnetic band filling per site  $n \leq 1$  only this band will be non-empty.

## B. Perturbative derivation of the effective magnon Hamiltonian.

At this stage, we will describe the perturbative treatment performed to derive the effective second-order Hamiltonian for magnons. We begin by rearranging the Hamiltonian terms, splitting it into a basic part  $H_0$ , including the MFA redefined ‘‘bare’’ magnon and electron Hamiltonians of previous section, plus a ‘‘perturbation’’  $I$ , which includes the full transverse Kondo coupling term ( $I^\perp \equiv H_K^\perp$ ) and the scattering (i.e. non-diagonal in boson operators) part of the longitudinal Kondo coupling ( $I^z$ ) not considered so far.

Explicitly, we have  $H = H_0 + I = H_0 + I^z + I^\perp$  where  $H_0 = \bar{H}_{Heis} + \bar{H}_{band}^{AF}$ . The longitudinal perturbation  $I^z$  reads:

$$\begin{aligned} I^z &= \frac{J_K}{N} \sum_{pqr,\sigma} (1 - \delta_{pq}) M_{r,p+r-q}^{++} \times \\ &\times (A_{r\sigma}^\dagger A_{p+r-q,\sigma} - B_{r\sigma}^\dagger B_{p+r-q,\sigma}) G_{pq} \\ &- \frac{J_K}{N} \sum_{pqr,\sigma} \sigma (1 - \delta_{pq}) L_{r,p+r-q}^{++} \times \\ &\times (A_{r\sigma}^\dagger B_{p+r-q,\sigma} + B_{r\sigma}^\dagger A_{p+r-q,\sigma}) G_{pq} \quad (32) \end{aligned}$$

The spin wave operators are contained in

$$\begin{aligned} G_{pq} &= a_p^\dagger a_q \text{Ch}(\vartheta_q) \text{Ch}(\vartheta_p) + a_{-q}^\dagger a_{-p} \text{Sh}(\vartheta_q) \text{Sh}(\vartheta_p) \\ &+ a_p^\dagger a_{-q}^\dagger \text{Sh}(\vartheta_q) \text{Ch}(\vartheta_p) + a_{-p} a_q \text{Ch}(\vartheta_q) \text{Sh}(\vartheta_p) \end{aligned}$$

while coefficients  $M_{r,p+r-q}^{++}$  and  $L_{r,p+r-q}^{++}$  are defined in the Appendix.

The transverse perturbation is written as:

$$\begin{aligned} I^\perp &= J_K \sqrt{\frac{S}{2}} \sum_q \left\{ [a_q^\dagger \text{Ch}(\vartheta_q) + a_{-q} \text{Sh}(\vartheta_q)] (s_{qA}^+ + s_{qB}^-) \right. \\ &\left. + [a_q^\dagger \text{Sh}(\vartheta_q) + a_{-q} \text{Ch}(\vartheta_q)] (s_{-qB}^+ + s_{-qA}^-) \right\} \quad (33) \end{aligned}$$

The spin operators are expressed through the electron operators as:

$$\begin{aligned} s_{qA}^\lambda + s_{qB}^\tau &= \\ &= \frac{1}{2} \sqrt{\frac{2}{N}} \sum_{k\sigma} A_{k\sigma}^\dagger A_{k+q,-\sigma} \mathcal{C}_{AA}^{\lambda\tau}(k, q) \\ &+ \frac{1}{2} \sqrt{\frac{2}{N}} \sum_{k\sigma} B_{k\sigma}^\dagger B_{k+q,-\sigma} \mathcal{C}_{BB}^{\lambda\tau}(k, q) \\ &+ \frac{1}{2} \sqrt{\frac{2}{N}} \sum_{k\sigma} \sigma A_{k\sigma}^\dagger B_{k+q,-\sigma} \mathcal{C}_{AB}^{\lambda\tau}(k, q) \\ &+ \frac{1}{2} \sqrt{\frac{2}{N}} \sum_{k\sigma} \sigma B_{k\sigma}^\dagger A_{k+q,-\sigma} \mathcal{C}_{BA}^{\lambda\tau}(k, q) \quad (34) \end{aligned}$$

where  $\lambda, \tau = \pm$  and the coefficients  $\mathcal{C}_{XY}^{\lambda\tau}(k, q)$  with  $X, Y = A, B$  are defined in the Appendix.

In the previous section, we have included at MFA level the effects of the diagonal part of the longitudinal Kondo coupling on the bosonic states (Eqs. 19-20) and on the AF electronic states (Eqs. 30-31). We will now determine the magnon renormalization effects derived from the transverse and non-diagonal parts of the longitudinal Kondo coupling, which we are considering as the perturbation  $I$  on the MFA state.

The effect of the perturbation will be taken into account through a Fröhlich-type of truncated unitary transformation<sup>24</sup>. We determine the generator  $R$  of an appropriate canonical transformation by eliminating the first order term in the perturbation. To this aim, we impose  $I + i[R, H_0] = 0$ . Introducing the notation  $\mathcal{R} \equiv \mathcal{R}^z + \mathcal{R}^\perp$ , we decompose this constraint into two separate equations, which can be solved yielding:  $\mathcal{R}^{z(\perp)} = \lim_{t \rightarrow 0} \frac{i}{\hbar} \int_{-\infty}^t I^{z(\perp)}(x) dx$ . By this procedure,<sup>25</sup> we obtain the second order effective Hamiltonian for the magnon-conduction electron system as:

$$\begin{aligned} H_{eff} &= \bar{H}_{band}^{AF} + \bar{H}_{Heis} + \frac{1}{2} [\mathcal{R}^z + \mathcal{R}^\perp, I^z + I^\perp] \\ &+ \mathcal{O}(I^z + I^\perp)^3, \quad (35) \end{aligned}$$

Let us remark here that the perturbative parameter which actually controls this expansion, is the ratio  $J_K/J_H$  weighed by factors(coefficients) which depend on the electronic band structure and filling, as can be seen from the explicit expressions for  $I^z$  and  $I^\perp$  given above. These electronic coefficients effectively reduce the magnitude of the perturbative control parameter from the raw value  $J_K/J_H$ , leading to a smooth convergence of the perturbative expansion even when  $|J_K/J_H|$  is near or exceeds one. This will become clear when we present our results for the renormalized magnons in next section.

Each term in the perturbation produces a corresponding term in the generator. From  $I^z$  we obtain the ‘‘longitudinal’’ generator  $R^z$  while from  $I^\perp$  we obtain the ‘‘transverse’’ generator  $R^\perp$ , which are conveniently de-

composed as:

$$R^z = \sum_{X,Y=A,B} \sum_{m=1,4} R_{mXY}^z \quad R^\perp = \sum_{X,Y=A,B} R_{XY}^\perp \quad (36)$$

The terms  $R_{mXY}^z$  and  $R_{XY}^\perp$  are detailed in the Appendix.

Finally, we make a projection onto the AF fermion wavefunction to obtain a second-order effective Hamiltonian for the magnons  $H_{SW}^{eff}$ . When taking the average  $\langle H_{eff} \rangle_{Fermi}$  over the AF Fermi wavefunction we find

$$\langle [\mathcal{R}^z, I^\perp] \rangle_{Fermi} = \langle [\mathcal{R}^\perp, I^z] \rangle_{Fermi} = 0 \quad (37)$$

so that the effective spin wave Hamiltonian has the sim-

pler form

$$\begin{aligned}
H_{SW}^{eff} &\equiv \langle H_{eff} \rangle_{Fermi} = \\
&= \sum_{k\sigma} (\mathcal{E}_{k\sigma}^A \langle n_{k\sigma}^A \rangle + \mathcal{E}_{k\sigma}^B \langle n_{k\sigma}^B \rangle) + \sum_q \hbar \Omega_q a_q^\dagger a_q \\
&\quad + \frac{1}{2} \langle [\mathcal{R}^z, I^z] + [\mathcal{R}^\perp, I^\perp] \rangle_{Fermi} \quad (38)
\end{aligned}$$

where

$$\langle n_{k\sigma}^X \rangle = [\exp(\mathcal{E}_{k\sigma}^X - \mu) / k_B T + 1]^{-1} \quad (39)$$

Evaluating  $\frac{1}{2} \langle [\mathcal{R}^z, I^z] + [\mathcal{R}^\perp, I^\perp] \rangle_{Fermi}$  we arrive at:

$$\begin{aligned}
H_{SW}^{eff} &= \sum_q \hbar (\Omega_q + \Theta_q) a_q^\dagger a_q + \sum_q \hbar \Psi_q (a_q^\dagger a_{-q}^\dagger + a_q a_{-q}) \\
&\quad + \text{const.} \quad (40)
\end{aligned}$$

The coefficients  $\hbar \Theta_q$  and  $\hbar \Psi_q$  are given by long and complicated expressions, which we detail in the Appendix. Here we just point out that both the harmonic and the anharmonic parts in  $H_{SW}^{eff}$  have contributions from both longitudinal and transverse Kondo terms.

With one last Bogolyubov transformation, we diagonalize the effective Hamiltonian for the spin excitations, yielding:

$$\begin{aligned}
H_{SW}^{eff} &= \sum_q \hbar \left[ (\Omega_q + \Theta_q) \sqrt{1 - \frac{4\Psi_q^2}{(\Omega_q + \Theta_q)^2}} \right] a_q^\dagger a_q \\
&\equiv \sum_q \hbar \tilde{\Omega}_q a_q^\dagger a_q \quad (41)
\end{aligned}$$

where  $\tilde{\Omega}_q$  is the renormalized antiferromagnetic spin wave frequency.

### III. RESULTS AND DISCUSSION

In the previous section, we obtained a formally simple final expression for the renormalized antiferromagnetic magnons in Eq. (41), but which depends on a series of coefficients which are detailed in the Appendix. The long complicated expressions for these perturbatively obtained coefficients, depend on the combined effect or interplay of the different model parameters: in particular, some coefficients involve double and triple summations, over the reduced Brillouin zone, of q-dependent filling factors of the conduction electron bands. Therefore, we have evaluated our renormalized magnon results numerically, exploring wide ranges of the different model parameters. This has allowed us not only to assess and compare the influence and main effect of each of the different model parameters, and show that one can reasonably explain experimental magnon results<sup>20,21</sup> employing parameters in the range independently shown to be appropriate for a phenomenological fit of specific heat measurements in this family of antiferromagnetic heavy

fermions,<sup>26</sup> as we will show below. Our exploration of wide parameter ranges has also allowed us to verify that the convergence radius of the perturbative series which determines the magnon renormalization is much wider than one might naively have expected. As mentioned below Eq. (35), results to be shown in this section evidence that the actual ‘‘small parameter’’ controlling this perturbative expansion is not just the bare  $J_K/J_H$  ratio: this appears weighed by electronic structure and filling dependent coefficients which effectively reduce the control parameter value from this ratio, leading to convergent magnon renormalization results for  $|J_K/J_H| > 1$ , when combined with suitable values of the other model parameters.

The numerical study of our model has been done assuming two simple cubic interpenetrating magnetic sublattices, for simplicity and without much loss of generality (rigorously, under this assumption our results would correspond to a cubic (bcc) lattice). Notice that  $\text{CeIn}_3$ ,<sup>21</sup> one of the compounds where inelastic neutron scattering (INS) on single crystals has measured the magnons we aim to describe, is cubic (though fcc) and has a three-dimensional Néel-type antiferromagnetic structure. We evaluated magnon excitations at zero temperature, and assuming an underlying 3D Néel-type antiferromagnetic ground state of the system: our study focuses on parameter sets far away from the quantum critical region of these systems, deep inside the antiferromagnetic phase. In fact, our parameters lie well inside the AF stable region recently determined by a DMFT + NRG study<sup>27</sup> of the magnetic phase diagram of the correlated Kondo-lattice (corresponding to the  $J_H = 0$  case of our model: the addition of non-negligible AF-like RKKY coupling  $J_H$ , as done here, will only increase the stability of the AF phase). As expt. observed,<sup>21</sup> in this range one might expect Kondo-type spin fluctuations to be less relevant and the dispersive spin waves, object of our study, to appear in the AF phase. In accordance with expt. indications<sup>21</sup> and for simplicity, we will further assume there is one isolated crystal field level of  $\text{Ce}^{3+}$  which is relevant, hosting a spin  $S = 1/2$  (in fact,  $m = 0.5\mu_B$  is the exp. magnitude of the local moments in  $\text{CeIn}_3$ <sup>21</sup>), and concentrate on the numerical evaluation of the renormalized spin waves given by Eq. (41). Hopping parameter  $t$  is taken as unit of energy, being  $W = 12t$  the total bare electron bandwidth.

In the following, we will start by exhibiting and discussing the general trends we have found in our study of magnon renormalization in the Heisenberg-Kondo model with a correlated conduction band. We shall end this section by focusing on the description of the measured magnons in antiferromagnetic heavy fermion compounds.

Fig. (1) depicts the first Brillouin zone (BZ) of the simple cubic lattice, and we include the notation for the special symmetry points and BZ paths on which the spin waves were numerically evaluated ( $\Gamma \equiv O$  denotes the zone center,  $\Delta \equiv X = 0.5\pi/a(1, 0, 0)$ ,  $Y = 0.5\pi/a(0, 1, 0)$ ,  $Z = 0.5\pi/a(0, 0, 1)$ ). Let us mention

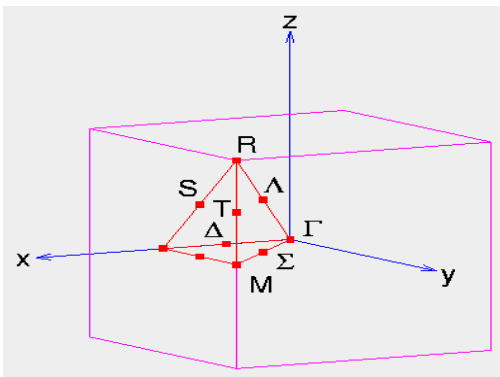


FIG. 1: Simple cubic lattice: 1st Brillouin zone and special symmetry points.

here that for the BZ summations we have used the special points BZ sampling method by Chadi-Cohen (CC), at 4th order, for the simple cubic lattice.<sup>28</sup> To obtain dressed magnons with the correct symmetry of the lattice, we have noticed<sup>25</sup> it is not sufficient to use the basic set of wave vectors of the (reduced) 1st BZ octant, but one needs to extend it to the (reduced) full 1st BZ (to properly take into account points at the frontiers between octants): we do this applying the (48) symmetry operations of the  $O_h$  group to the basic set. Thus, at 4th-order CC, taking into account all symmetry operations we have included 5760 special symmetry points for each BZ summation. To achieve higher accuracy for our determination of the Fermi level (a delicate issue close to half-filling), we have used integration over the 5th order Chadi-Cohen vectors ( that is, we used 39168 special symmetry points taking all symmetry operations into account).

In Fig. (2) we show the typical conduction electron bandstructure near half-filling, given by Eq. (30), obtained with the variational approach described in section (II A). Notice that for each value of  $U$  only the lower band (denoted  $A$ ) is filled. Chemical potential values obtained for the four cases shown are:  $\mu/t = -0.63, 0.58, 0.49, 0.18$ , (slightly below the top of the lowest band), respectively for  $U/W = 0.008, 0.25, 0.5, 0.83$  [ i.e.  $U/t$  values of Fig. (2) ]. We obtain a direct band gap, determined by the AF subband energies at the cube diagonal BZ point:  $q = R$  (see Fig. (1) ). As expected, the size of the gap, as well as the energy of its centroid, increase with electron correlation ( $U$ ) magnitude, while also a correlation-driven band narrowing effect is being described. The AF band gap value essentially depends on  $U \langle s \rangle$ , with  $\langle s \rangle$  growing with both the band filling  $n$  and correlation  $U$ . In Table I these trends of the AF band polarization with the different parameters are recognized. It is also interesting to compare our AF band polarization values (tabulated) with those reported in Fig.2 of Ref. [27], for corresponding parameters. Notwithstanding the different respective treatments for the band electron correlations, we find quite reasonable agreement where

we could check it: in the present work we have used antiferromagnetic Kondo coupling values in a relatively narrow region around AF  $J_K/W \sim 10^{-5} - 10^{-3}$ . In agreement with Peters and Pruschke,<sup>27</sup> in this parameter range we find that the local moments are almost fully polarized, while the corresponding band polarization obtained for  $U \sim 0$  and  $U \sim W$  agrees quite well with the corresponding values in Fig.2 of Ref. [27].

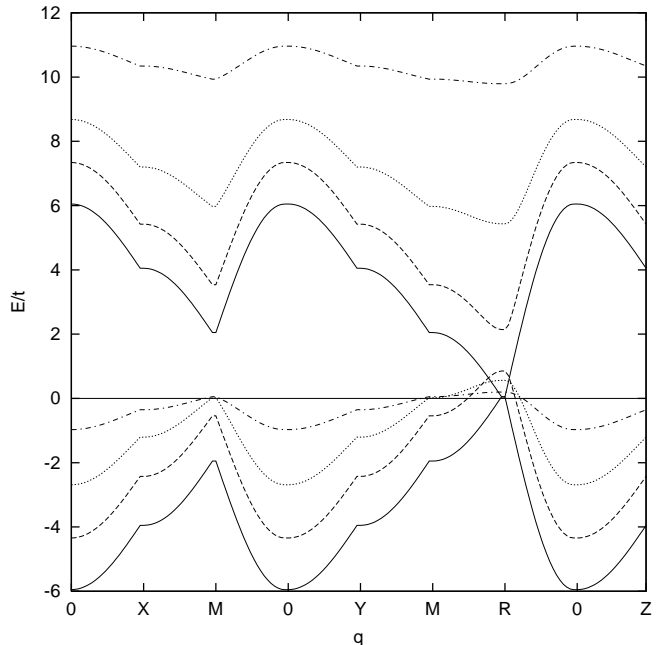


FIG. 2: Hybridized electron bands ( $\uparrow$ ) along selected BZ paths. Parameters:  $S = 1/2; T = 0; t = 1eV; J_H/t = 0.001; J_K/J_H = 1; n = 0.999$ .  $U/t = 0.1$  (full lines), 3 (dashed), 6 (dotted), 10 (dash-dotted).

In Fig. (3) we show the dependence of the AF magnon renormalization on the bare  $J_K/J_H$  ratio at half-filling ( the most relevant filling for AF heavy fermion compounds): the lowest curve represents the bare magnons  $\omega_q$  (independent of the conduction electrons). As a general trend, we find that the renormalization effects beyond mean-field approximation reduce the spin wave frequency  $\tilde{\Omega}_q$  with respect to the MFA value  $\Omega_q$ , but still the total renormalization effect  $\omega_q \implies \tilde{\Omega}_q$  is a hardening with respect to the bare (non-interacting) magnon frequency:  $\omega_q < \tilde{\Omega}_q < \Omega_q$ . It is reasonable that due to their coupling to the conduction electrons, magnon excitations in the coupled magnetic system require a larger energy than when the excitation involves only the local moment subsystem. Thus, the dressed magnon energies increase with respect to the bare ones in an amount proportional to the increase in relative weight of the Kondo coupling with respect to the bare RKKY (Heisenberg) coupling, as Fig. (3) shows. Meanwhile,  $zJ_H S$  sets the main energy scale for the magnons. On the other hand, the renormalization due to only mean-field approximation effects is a hardening with respect to bare magnons: notice that the

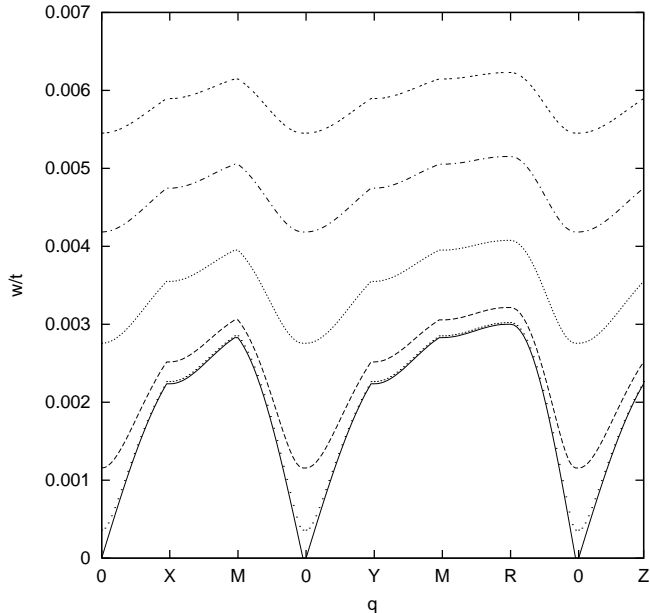


FIG. 3:  $J_k/J_H$  dependence of renormalized AF magnons: magnon energy along selected BZ paths. Parameters:  $S = 1/2$ ;  $T = 0$ ;  $t = 1eV$ ;  $J_H/t = 0.001$ ;  $n = 0.999$ ;  $U/t = 3$ . Full line: bare AF magnons.  $J_K/J_H = 0.1$  (sparsely dotted line), 1 (dashed), 5 (densely dotted), 10 (dash-dotted), 15 (double-dashed).

MFA of the longitudinal part of the Kondo interaction employed here, leads to a factor of  $zJ_H S + |J_K < s >|$  for the “MFA-renormalized” frequency, from which the (longitudinal) Kondo coupling is seen to induce a magnon hardening: which is partially reduced when the full renormalization effects are taken into account.

Next figure ( Fig. (4) ) depicts the dependence of the renormalized magnons on the correlations in the conduction band ( $U$ ), at half-filling: the trend is a hardening of magnons when  $U$  is increased ( such hardening appears also for the MFA magnons), and we show cases where  $U/W$  ranges between 0.008 (for  $U/t = 0.1$ ) and 0.83 ( $U/t = 10$ ). This may be understood by the reinforcement of  $U$ -dependent antiferromagnetism (spin polarization) in the conduction band, which renders conduction electrons less available to follow easily the spin excitation determined by magnon excitation in the local moment subsystem: an energetic cost is involved. In fact, the magnon gap value we obtain at  $q = 0$  is directly related to the correlation value, and to the symmetry breaking involved in our treatment when the itinerant antiferromagnetism of the conduction band is considered ( as was also reported in previous work on spin excitations in manganites).<sup>29</sup> Notice that increasing  $U$  also reduces  $q$ -dependent details in the renormalized magnons: this can be explained by analyzing the indirect effect which  $U$  has on magnons (while  $J_K$  has also a direct effect, since it appears also as explicit multiplicative factor of

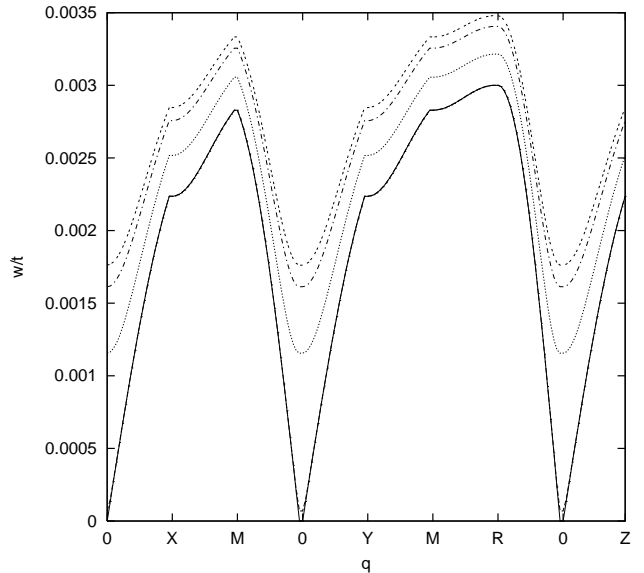


FIG. 4:  $U$  dependence of renormalized AF magnons: magnon energy along selected BZ paths. Parameters:  $U$  as detailed here; others as in Fig. 2. Full line: bare AF magnons.  $U/t = 0.1$  (sparse dots: indiscernible from bare magnon curve in plot), 1 (dashed line), 3 (densely dotted), 6 (dash-dotted) , 10 (double-dashed).

the perturbatively obtained magnon corrections).  $U$  affects magnons through the modifications it induces in electron bandstructure, and in particular the  $U$ -driven increase of energy denominators of the perturbative coefficients which determine the  $q$ -dependent renormalization of magnons (details in the Appendix), which explains the above mentioned result. The recent more refined DMFT+NRG treatment of correlations in an extended Kondo lattice model<sup>27</sup> unfortunately does not allow us comparison, here, as their finite  $U$  results are presented for antiferromagnetic  $J_K$  outside the region of interest in our problem: their correlated AF Kondo coupling system is studied at much too large Kondo coupling (namely,  $J_K = 0.5W = U$ ) for the antiferromagnetic state to remain stable, being the Kondo insulator with all moments locally quenched the stable phase near half filling in that case.

We exhibit effects of the doping on the magnon renormalization in Fig. (5). Here the deviation of the renormalized magnon energies from the bare magnon values is increased with the filling: at half-filling the renormalization is largest, there being more conduction electrons present, which contribute to the renormalization of magnons by their Kondo coupling to the local moments. Doping away from half-filling we obtain a smooth reduction of such renormalization effects. Thus, both filling and electron correlation do increase renormalization effects, and we have already mentioned that both result in similar increases of spin polarization of the conduction band. We will shortly come back to this point, when



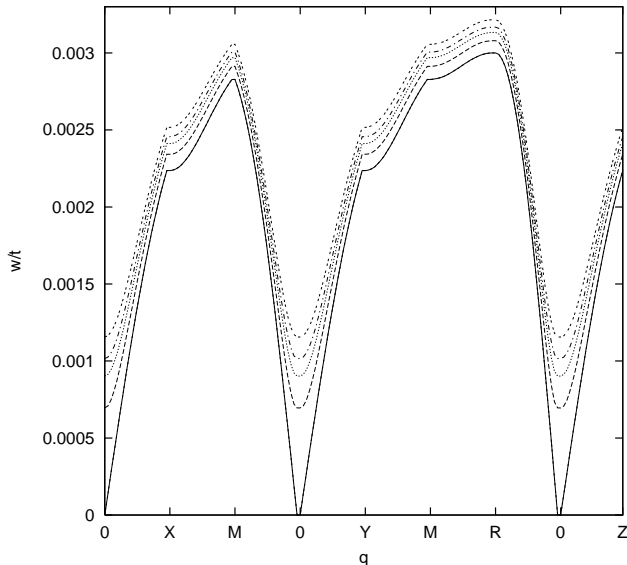


FIG. 5: Filling ( $n$ ) dependence of renormalized AF magnons: magnon energy along selected BZ paths. Parameters:  $U/t = 3$ ;  $n$  as detailed here; others as in Fig. 2. Full line: bare AF magnons.  $n = 0.999$  (double-dashed line), 0.8 (dash-dotted), 0.7 (dotted), 0.6 (dashed), 0.4 (sparsely dotted line: indiscernible from bare magnon curve in plot).

introducing our last figure.

Let us briefly refer again to the  $q$ -dependence of the AF magnon renormalization we find. Some anisotropy is present: a larger  $q$ -dependence is noticeable along BZ diagonal paths such as  $O-M$  or  $O-R$  (see e.g. Fig. (5)) or paths along the symmetry axes. While the renormalization effects are more pronounced at long wavelengths: in particular, they are maximal at the BZ center where we find a spin stiffness increasing with doping, and decreasing with  $U$  or  $J_K/J_H$ . Making allowance for the quite different systems involved, let us mention that the renormalized AF magnon behavior we obtain contrasts with the one recently disclosed by INS measurements in *ferromagnetic metallic manganites*:<sup>30</sup> where low- $q$  spin wave stiffness appears insensitive to doping, while magnons exhibit a doping-dependent renormalization at the BZ boundaries (recently suggested to be related to electronic correlations<sup>31</sup>).

At this point, let us compare our results with the few INS magnon measurements available for single crystals of antiferromagnetic heavy fermions. Comparison in more detail may be made only with  $\text{CeIn}_3$ , which is cubic (though f.c.c.) and presents a three-dimensional AF order as we have assumed for our calculation. In Fig. (6) we show magnon results we obtained with three different sets of model parameters: as can be seen, all of them providing a reasonably good description of the measured  $\text{CeIn}_3$  magnons.<sup>21</sup> At the same time, these parameter sets yield examples of behavior of the magnon renormalization of the model discussed above:

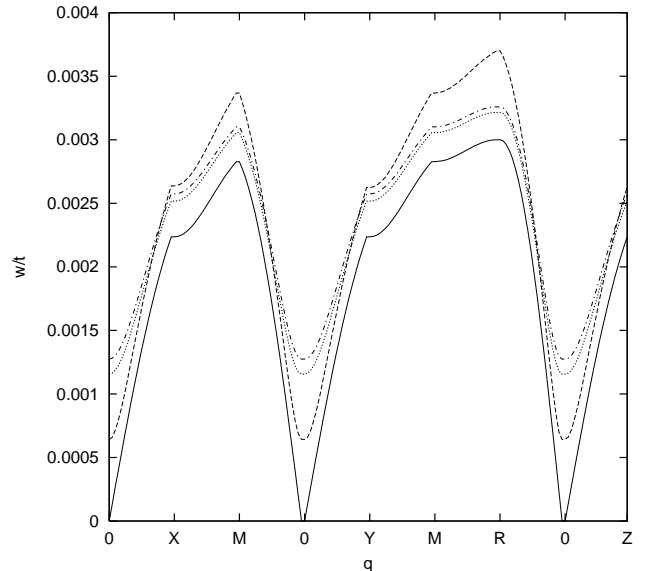


FIG. 6: Three parameter sets leading to renormalized AF magnons as in  $\text{CeIn}_3$ . (a):  $J_K/J_H = 100$ ,  $U/t = 0.001$ ,  $n = 0.999$  (bare magnons: full line; ren. magnons: dashed); (b):  $J_K/J_H = 1$ ,  $U/t = 3$ ,  $n = 0.999$  (dotted); (c):  $J_K/J_H = 1$ ,  $U/t = 6$ ,  $n = 0.7$  (dash-dotted). Other parameters as Fig. 2.

(a) the first parameter set used in Fig. 6 provides an example of convergence of our perturbative expansion for a case with  $J_K > J_H (= 100J_H)$ , at half-filling and with negligible  $U$ ; notice a slightly larger  $q$ -dependence is obtained in this case (to be expected from the  $q$ -dependent expressions of the perturbative coefficients): e.g. easily noticeable different height of the main peaks (at symmetry points M and R) is visible;

(b) with parameter set (b) of Fig. 6, again a reasonable qualitative description of expt.  $\text{CeIn}_3$  magnons is obtained (considering our calculations are done for sc magnetic sublattices (thus bcc lattice), while  $\text{CeIn}_3$  in fact is fcc). The agreement here is slightly better than with set (a). This shows how delicate the interplay between the different parameters of the model is: since, compared with parameter set (a), here we obtain a quite similar result at half-filling but with  $J_K = J_H$  and  $U/t = 3$ ;

(c) finally we illustrate that we can obtain a quite similar description of the  $\text{CeIn}_3$  measured magnons away from half filling: e.g. assuming  $n = 0.7$  but compensating the decrease in electron energy due to doping by an increase in band correlation: taking  $U/t = 6$  while keeping  $J_K = J_H$ .

It is also worth mentioning that these sets of parameters allowing description of INS results are in parameter ranges independently suggested by other authors for these compounds. A concrete example is the phenomenological fit of specific heat curves for  $\text{CeIn}_3$ , which was made by Lobos et al.,<sup>26</sup> using:  $J_H/t = 0.0014$ ,  $t = 0.5eV$ ,  $n = 1$  and  $J_K/J_H = 980$ ; while for  $\text{CeRh}_2\text{Si}_2$  they have used:  $J_H/t = 0.0034$  and  $J_K/J_H = 430$ ; and their data

extrapolation for CePd<sub>2</sub>Si<sub>2</sub> was:  $J_H/t = 0.0034$  with a negligible  $J_K/J_H$ .

#### IV. SUMMARY

In the present work, we have studied spin wave excitations in heavy fermion compounds with antiferromagnetic long-range order, where a strong competition of RKKY and Kondo screening is present, as evidenced by nearly equal magnetic ordering and Kondo temperatures. We have described these systems using a microscopic model including a lattice of correlated f-electron orbitals (as in Ce-, U- compounds of this family) hybridized with a correlated conduction band, with the presence of competing RKKY-Heisenberg and Kondo magnetic couplings.

Through a series of unitary transformations we perturbatively derived a second-order effective Hamiltonian describing the spin wave excitations, renormalized by their interaction with the conduction electrons. We have numerically studied the effect of the different parameters of this effective model on the magnon energy renormalization by the conduction electrons.

We have been able to find appropriate sets of model parameters to describe the few existing measurements of magnons by inelastic neutron scattering in single crystal samples of antiferromagnetic heavy fermion Ce compounds. These parameter sets also agree with the ranges proposed for these compounds, through phenomenological fits of other experiments, like specific heat. Our results may provide information of interest for the prediction of inelastic neutron scattering experiments in other compounds of this family, like CeRh<sub>2</sub>Si<sub>2</sub>, where there have been suggestions that the RKKY coupling should be stronger than Kondo effect,<sup>15</sup> and the only existing NIS measurements are of poor quality: they were made on polycrystals<sup>15</sup> many years ago, and with lower resolution.

As outlook towards related future work, we might mention the description of the experimentally reported magnon damping effects, and the study of the coexistence of antiferromagnetism and superconductivity in the context of the present model.

#### Acknowledgments

We thank J. Sereni, E. Müller-Hartmann, G. Aeppli, P. Coleman, P. Gegenwart, P. Santini, A. Lobos, and J.R. Iglesias for discussions and references. M.A. thanks Centro Atómico Bariloche for the hospitality and support. C.I.V. is Investigador Científico of CONICET (Argentina), and acknowledges support from CONICET (PEI'6298 and PIP'5342 grants), Consiglio Nazionale delle Ricerche (CNR Short-Term Mobility Grant 2006), as well as hospitality and support from Dipto. di Fisica (Univ. di Parma), Inst. für Theoretische

Physik (Univ. zu Köln) and the International Centre for Theoretical Physics (ICTP, Trieste).

#### V. APPENDIX.

In Eq.32 the coefficients  $M_{r,p+r-q}^{++}$  and  $L_{r,p+r-q}^{++}$  are a particular case of  $L_{kp}^{\lambda\tau}, M_{kp}^{\lambda\tau}$  with  $\lambda, \tau = \pm$ , defined as:

$$\begin{aligned} L_{kp}^{\lambda\tau} &= \cos [\xi_k + \lambda\xi_p + \tau (\zeta_k + \lambda\zeta_p)] \\ M_{kp}^{\lambda\tau} &= \sin [\xi_k + \lambda\xi_p + \tau (\zeta_k + \lambda\zeta_p)] \end{aligned} \quad (42)$$

In Eq.33 the coefficients  $\mathcal{C}_{XY}^{\lambda\tau}(k, q)$  with  $X, Y = A, B$  are defined as:

$$\begin{aligned} \mathcal{C}_{XY}^{+-}(k, q) &= \delta_{XY} \left[ L_{k,k+q}^{++} + (1 - 2\delta_{XA}) M_{k,k+q}^{-+} \right] \\ &\quad + (1 - \delta_{XY}) \left[ L_{k,k+q}^{-+} + (1 - 2\delta_{XA}) M_{k,k+q}^{++} \right] \\ \mathcal{C}_{XX}^{-+}(k, q) &= \mathcal{C}_{YY}^{+-}(k, q) \quad \mathcal{C}_{XY}^{-+}(k, q) = -\mathcal{C}_{YX}^{+-}(k, q) \end{aligned} \quad (43)$$

From the longitudinal Kondo term  $I^z$  one obtains the generator  $R^z = \sum_{X,Y=A,B} \sum_{m=1,4} R_{mXY}^z$ , Eq.36, as the sum of sixteen contributions. By defining the bosonic operator

$$\mathfrak{R}_{mq} = \delta_{m1} a_p^\dagger a_q + \delta_{m2} a_{-q}^\dagger a_{-p} + \delta_{m3} a_p^\dagger a_{-q}^\dagger + \delta_{m4} a_{-p} a_q$$

we have

$$\begin{aligned} \mathcal{R}_{mXY}^z &= \sum_{pqr,\sigma} [\delta_{XY} + (1 - \delta_{XY}) \sigma] (1 - \delta_{pq}) \times \\ &\quad \times \mathcal{X}_{prq}^{mXY} X_{r\sigma}^\dagger Y_{p+r-q\sigma} \mathfrak{R}_{mq} \end{aligned} \quad (44)$$

The operators  $R_{mXY}^z$  depend on the coefficients  $\mathcal{X}_{pq\sigma}^{mXY}$ . Defining

$$F_{kpq}^{XY\lambda\tau} = \mathcal{E}_k^X - \mathcal{E}_{k+p-q}^Y + \lambda\hbar(\Omega_q + \tau\Omega_p)$$

we can write compactly

$$\begin{aligned} \mathcal{X}_{pkq}^{1XY} &= \delta_{XY} (1 - 2\delta_{XB}) \frac{M_{k,p-q+k}^{++}}{F_{kpq}^{XX+-}} \text{Ch}(\vartheta_q) \text{Ch}(\vartheta_p) \\ &\quad - (1 - \delta_{XY}) \frac{L_{k,p-q+k}^{++}}{F_{kpq}^{XY+-}} \text{Ch}(\vartheta_q) \text{Ch}(\vartheta_p) \end{aligned} \quad (45)$$

$$\begin{aligned} \mathcal{X}_{pkq}^{2XY} &= \delta_{XY} (1 - 2\delta_{XB}) \frac{M_{k,p-q+k}^{++}}{F_{kpq}^{XX+-}} \text{Sh}(\vartheta_q) \text{Sh}(\vartheta_p) \\ &\quad - (1 - \delta_{XY}) \frac{L_{k,p-q+k}^{++}}{F_{kpq}^{XY+-}} \text{Sh}(\vartheta_q) \text{Sh}(\vartheta_p) \end{aligned} \quad (46)$$

$$\begin{aligned} \mathcal{X}_{pkq}^{3XY} &= \delta_{XY} (1 - 2\delta_{XB}) \frac{M_{k,p-q+k}^{++}}{F_{kpq}^{XX++}} \text{Sh}(\vartheta_q) \text{Ch}(\vartheta_p) \\ &\quad - (1 - \delta_{XY}) \frac{L_{k,p-q+k}^{++}}{F_{kpq}^{XY++}} \text{Sh}(\vartheta_q) \text{Ch}(\vartheta_p) \end{aligned} \quad (47)$$

$$\begin{aligned} \mathcal{X}_{pkq}^{4XY} &= \delta_{XY} (1 - 2\delta_{XB}) \frac{M_{k,p-q+k}^{++}}{F_{kpq}^{XX--}} \text{Sh}(\vartheta_q) \text{Ch}(\vartheta_p) \\ &\quad - (1 - \delta_{XY}) \frac{L_{k,p-q+k}^{++}}{F_{kpq}^{XY--}} \text{Sh}(\vartheta_q) \text{Ch}(\vartheta_p) \end{aligned} \quad (48)$$

The generator  $R^\perp$  resulting from the transverse Kondo term  $I^\perp$ , Eq.36, has four contributions:  $\mathcal{R}^\perp = \sum_{X,Y=A,B} \mathcal{R}_{XY}^\perp$ , namely:

$$\begin{aligned} \mathcal{R}_{XY}^\perp &= \frac{J_K}{2} \sqrt{\frac{S}{N}} \sum_{kq\sigma} [\delta_{XY} + (1 - \delta_{XY}) \sigma] \times \\ &\quad \times X_{k\sigma}^\dagger Y_{k+q,-\sigma} (\mathcal{W}_{kq}^{XY} a_q^\dagger + \mathcal{Z}_{kq}^{XY} a_{-q}) \end{aligned} \quad (49)$$

The coefficients  $\mathcal{W}_{kq}^{XY}$  and  $\mathcal{Z}_{kq}^{XY}$  are given by:

$$\mathcal{W}_{kq}^{XY} = \frac{[\text{Ch}(\vartheta_q) \mathcal{C}_{XY}^{+-}(k, q) + \text{Sh}(\vartheta_q) \mathcal{C}_{XY}^{-+}(k, q)]}{(\mathcal{E}_k^X - \mathcal{E}_{k+q}^Y + \hbar\Omega_q)} \quad (50)$$

$$\mathcal{Z}_{kq}^{XY} = \frac{[\text{Sh}(\vartheta_q) \mathcal{C}_{XY}^{+-}(k, q) + \text{Ch}(\vartheta_q) \mathcal{C}_{XY}^{-+}(k, q)]}{(\mathcal{E}_k^X - \mathcal{E}_{k+q}^Y - \hbar\Omega_q)} \quad (51)$$

We have obtained the effective Hamiltonian in Eq.38. The contribution from the perturbations  $\frac{1}{2} \langle [\mathcal{R}, I] \rangle_{fermi}$  can be written as the sum of four terms:

$$\begin{aligned} &\frac{1}{2} \langle [\mathcal{R}, I] \rangle_{fermi} \\ &= \frac{1}{2} \sum_q \sum_{X,Y=A,B} \mathcal{T}_q^{XY} a_q^\dagger a_q \\ &\quad + \frac{1}{4} \sum_q \sum_{X,Y=A,B} (\mathcal{S}_q^{XY1} + \mathcal{S}_q^{XY2}) (a_q^\dagger a_{-q}^\dagger + a_q a_{-q}) \\ &\quad + \frac{1}{2} \sum_q \hbar (\mathcal{D}_q^{z+} + \mathcal{D}_q^{z-}) a_q^\dagger a_q \\ &\quad + \frac{1}{4} \sum_q \hbar (\varpi_q^{z+} + \varpi_q^{z-}) (a_q^\dagger a_{-q}^\dagger + a_q a_{-q}) \end{aligned} \quad (52)$$

Assuming the paramagnetic band filling per site  $n \leq 1$  so that  $\langle n_{k,\sigma}^B \rangle = 0$  in the ground state, one finds  $\mathcal{T}_q^{BB} = \mathcal{S}_q^{BB} = 0$ .

The  $\mathcal{T}_q^{XY}$  coefficients, by defining  $\langle N_{k,\pm q,\sigma} \rangle = \langle n_{k,-\sigma}^A \rangle - \langle n_{k\pm q,\sigma}^A \rangle$ , read:

$$\begin{aligned} \mathcal{T}_q^{AA} &= \frac{J_K^2 S}{4N} \sum_{k\sigma} \mathcal{W}_{k,q}^{AA} \text{Sh}(\vartheta_q) \mathcal{C}_{AA}^{+-}(k+q, -q) \langle N_{k,+q,\sigma} \rangle \\ &\quad + \frac{J_K^2 S}{4N} \sum_{k\sigma} \mathcal{W}_{k,q}^{AA} \text{Ch}(\vartheta_q) \mathcal{C}_{BB}^{+-}(k+q, -q) \langle N_{k,+q,\sigma} \rangle \\ &\quad + \frac{J_K^2 S}{4N} \sum_{k\sigma} \mathcal{Z}_{k,-q}^{AA} \text{Ch}(\vartheta_q) \mathcal{C}_{AA}^{+-}(k-q, q) \langle N_{k,-q,\sigma} \rangle \\ &\quad + \frac{J_K^2 S}{4N} \sum_{k\sigma} \mathcal{Z}_{k,-q}^{AA} \text{Sh}(\vartheta_q) \mathcal{C}_{BB}^{+-}(k-q, q) \langle N_{k,-q,\sigma} \rangle \end{aligned} \quad (53)$$

$$\begin{aligned} \mathcal{T}_q^{AB} &= -\frac{J_K^2 S}{2N} \sum_{k\sigma} \mathcal{W}_{k,q}^{AB} \text{Sh}(\vartheta_q) \mathcal{C}_{BA}^{+-}(k+q, -q) \langle n_{k,-\sigma}^A \rangle \\ &\quad + \frac{J_K^2 S}{2N} \sum_{k\sigma} \mathcal{W}_{k,q}^{AB} \text{Ch}(\vartheta_q) \mathcal{C}_{AB}^{+-}(k+q, -q) \langle n_{k,-\sigma}^A \rangle \\ &\quad - \frac{J_K^2 S}{2N} \sum_{k\sigma} \mathcal{Z}_{k,-q}^{AB} \text{Ch}(\vartheta_q) \mathcal{C}_{BA}^{+-}(k-q, q) \langle n_{k,-\sigma}^A \rangle \\ &\quad + \frac{J_K^2 S}{2N} \sum_{k\sigma} \mathcal{Z}_{k,-q}^{AB} \text{Sh}(\vartheta_q) \mathcal{C}_{AB}^{+-}(k-q, q) \langle n_{k,-\sigma}^A \rangle \end{aligned} \quad (54)$$

and

$$\begin{aligned} \mathcal{T}_q^{BA} &= \frac{J_K^2 S}{2N} \sum_k \mathcal{W}_{k,q}^{BA} \text{Sh}(\vartheta_q) \mathcal{C}_{AB}^{+-}(k+q, -q) \langle n_{k+q,\sigma}^A \rangle \\ &\quad - \frac{J_K^2 S}{2N} \sum_k \mathcal{W}_{k,q}^{BA} \text{Ch}(\vartheta_q) \mathcal{C}_{BA}^{+-}(k+q, -q) \langle n_{k+q,\sigma}^A \rangle \\ &\quad + \frac{J_K^2 S}{2N} \sum_k \mathcal{Z}_{k,-q}^{BA} \text{Ch}(\vartheta_q) \mathcal{C}_{AB}^{+-}(k-q, q) \langle n_{k-q,\sigma}^A \rangle \\ &\quad - \frac{J_K^2 S}{2N} \sum_k \mathcal{Z}_{k,-q}^{BA} \text{Sh}(\vartheta_q) \mathcal{C}_{BA}^{+-}(k-q, q) \langle n_{k-q,\sigma}^A \rangle \end{aligned} \quad (55)$$

The  $\mathcal{S}_q^{XY1}$  coefficients read:

$$\begin{aligned} \mathcal{S}_q^{AA1} &= \frac{J_K^2 S}{2N} \sum_k \mathcal{W}_{k,-q}^{AA} \text{Ch}(\vartheta_q) \mathcal{C}_{AA}^{+-}(k-q, q) \langle N_{k,-q,\sigma} \rangle \\ &\quad + \frac{J_K^2 S}{2N} \sum_k \mathcal{W}_{k,-q}^{AA} \text{Sh}(\vartheta_q) \mathcal{C}_{BB}^{+-}(k-q, q) \langle N_{k,-q,\sigma} \rangle \end{aligned} \quad (56)$$

$$\begin{aligned} \mathcal{S}_q^{AB1} &= -\frac{J_K^2 S}{2N} \sum_k \mathcal{W}_{k,-q}^{AB} \text{Ch}(\vartheta_q) \mathcal{C}_{BA}^{+-}(k-q, q) \langle n_{k,-\sigma}^A \rangle \\ &\quad + \frac{J_K^2 S}{2N} \sum_k \mathcal{W}_{k,-q}^{AB} \text{Sh}(\vartheta_q) \mathcal{C}_{AB}^{+-}(k-q, q) \langle n_{k,-\sigma}^A \rangle \end{aligned} \quad (57)$$

$$\begin{aligned} \mathcal{S}_q^{BA1} &= \frac{J_K^2 S}{2N} \sum_k \mathcal{W}_{k,-q}^{BA} \text{Ch}(\vartheta_q) \mathcal{C}_{AB}^{+-}(k-q, q) \langle n_{k-q, \sigma}^A \rangle \\ &\quad - \frac{J_K^2 S}{2N} \sum_k \mathcal{W}_{k,-q}^{BA} \text{Sh}(\vartheta_q) \mathcal{C}_{BA}^{+-}(k-q, q) \langle n_{k-q, \sigma}^A \rangle \end{aligned} \quad (58)$$

The coefficients  $\mathcal{S}_q^{XY2}$  can be obtained from  $\mathcal{S}_q^{XY1}$  by interchanging  $\mathcal{W}_{k,-q}^{XY}$  and  $\text{Ch}(\vartheta_q)$  respectively with  $\mathcal{Z}_{k,-q}^{XY}$  and  $\text{Sh}(\vartheta_q)$ .

To write down the coefficients  $\mathcal{D}_q^{z\pm}$  and  $\varpi_q^{z\pm}$  of Eq.40 it is convenient to introduce:

$$\text{Ch}(\vartheta_q + \vartheta_p) = \mathfrak{C}_{qp} \quad \text{Sh}(\vartheta_q + \vartheta_p) = \mathfrak{S}_{qp}$$

By defining

$$\begin{aligned} \mathcal{L}_{pqr}^+ &= M_{r,p-q+r}^{++} (\mathcal{X}_{q,p-q+r,p}^{AA1} + \mathcal{X}_{-p,p-q+r,-q}^{AA2}) \mathfrak{C}_{qp} \langle n_{p-q+r,\sigma}^A \rangle \\ &\quad - L_{r,p-q+r}^{++} (\mathcal{X}_{q,p-q+r,p}^{AB1} + \mathcal{X}_{-p,p-q+r,-q}^{AB2}) \mathfrak{C}_{qp} \langle n_{p-q+r,\sigma}^A \rangle \\ &\quad - M_{r,p-q+r}^{++} (\mathcal{X}_{q,p-q+r,p}^{AA3} + \mathcal{X}_{-p,p-q+r,-q}^{AA4}) \mathfrak{S}_{qp} \langle n_{r\sigma}^A \rangle \\ &\quad + L_{r,p-q+r}^{++} (\mathcal{X}_{q,p-q+r,p}^{BA3} + \mathcal{X}_{-p,p-q+r,-q}^{BA4}) \mathfrak{S}_{qp} \langle n_{r\sigma}^A \rangle \end{aligned} \quad (59)$$

and

$$\begin{aligned} \mathcal{L}_{pqr}^- &= -M_{r,p-q+r}^{++} (\mathcal{X}_{-p,p-q+r,-q}^{AA1} + \tilde{\mathcal{X}}_{q,p-q+r,p}^{AA2}) \mathfrak{C}_{qp} \langle n_{r\sigma}^A \rangle \\ &\quad + L_{r,p-q+r}^{++} (\mathcal{X}_{-p,p-q+r,-q}^{BA1} + \mathcal{X}_{q,p-q+r,p}^{BA2}) \mathfrak{C}_{qp} \langle n_{r\sigma}^A \rangle \\ &\quad + M_{r,p-q+r}^{++} (\mathcal{X}_{q,p-q+r,p}^{AA4} + \mathcal{X}_{-p,p-q+r,-q}^{AA3}) \mathfrak{S}_{qp} \langle n_{p-q+r,\sigma}^A \rangle \\ &\quad - L_{r,p-q+r}^{++} (\mathcal{X}_{q,p-q+r,p}^{AB4} + \mathcal{X}_{-p,p-q+r,-q}^{AB3}) \mathfrak{S}_{qp} \langle n_{p-q+r,\sigma}^A \rangle \end{aligned} \quad (60)$$

we can write

$$\hbar \mathcal{D}_q^{z\pm} = \frac{J_K^2}{2} \left( \frac{2}{N} \right)^2 \sum_{pr} (1 - \delta_{pq}) \mathcal{L}_{pqr}^{\pm} \quad (61)$$

Next, by defining

$$\begin{aligned} \mathcal{G}_{pqr}^+ &= M_{r,p-q+r}^{++} (\mathcal{X}_{q,p-q+r,p}^{AA1} + \mathcal{X}_{-p,p-q+r,-q}^{AA2}) \mathfrak{S}_{qp} \langle n_{p-q+r,\sigma}^A \rangle \\ &\quad - L_{r,p-q+r}^{++} (\mathcal{X}_{q,p-q+r,p}^{AB1} + \mathcal{X}_{-p,p-q+r,-q}^{AB2}) \mathfrak{S}_{qp} \langle n_{p-q+r,\sigma}^A \rangle \\ &\quad - M_{r,p-q+r}^{++} (\mathcal{X}_{q,p-q+r,p}^{AA3} + \mathcal{X}_{-p,p-q+r,-q}^{AA4}) \mathfrak{C}_{qp} \langle n_{r\sigma}^A \rangle \\ &\quad + L_{r,p-q+r}^{++} (\mathcal{X}_{q,p-q+r,p}^{BA3} + \mathcal{X}_{-p,p-q+r,-q}^{BA4}) \mathfrak{C}_{qp} \langle n_{r\sigma}^A \rangle \end{aligned} \quad (62)$$

and

$$\begin{aligned} \mathcal{G}_{pqr}^- &= -M_{r,p-q+r}^{++} (\mathcal{X}_{-p,p-q+r,-q}^{AA1} + \mathcal{X}_{q,p-q+r,p}^{AA2}) \mathfrak{S}_{qp} \langle n_{r\sigma}^A \rangle \\ &\quad + L_{r,p-q+r}^{++} (\mathcal{X}_{-p,p-q+r,-q}^{BA1} + \mathcal{X}_{q,p-q+r,p}^{BA2}) \mathfrak{S}_{qp} \langle n_{r\sigma}^A \rangle \\ &\quad + M_{r,p-q+r}^{++} (\mathcal{X}_{q,p-q+r,p}^{AA4} + \mathcal{X}_{-p,p-q+r,-q}^{AA3}) \mathfrak{C}_{qp} \langle n_{p-q+r,\sigma}^A \rangle \\ &\quad - L_{r,p-q+r}^{++} (\mathcal{X}_{q,p-q+r,p}^{AB4} + \mathcal{X}_{-p,p-q+r,-q}^{AB3}) \mathfrak{C}_{qp} \langle n_{p-q+r,\sigma}^A \rangle \end{aligned} \quad (63)$$

we can write

$$\hbar \varpi_q^{z\pm} = \frac{J_K^2}{2} \left( \frac{2}{N} \right)^2 \sum_{pr} (1 - \delta_{pq}) \mathcal{G}_{pqr}^{\pm} \quad (64)$$

Using this set of contributions, the coefficients  $\Theta_q$  and  $\Psi_q$  in Eq.40 are defined as:

$$\hbar \Theta_q = \frac{1}{2} \sum_{X,Y=A,B} \mathcal{T}_q^{XY} + \frac{1}{2} (\hbar \mathcal{D}_q^{z+} + \hbar \mathcal{D}_q^{z-}) \quad (65)$$

$$\hbar \Psi_q = \sum_{X,Y=A,B} \left( \frac{\mathcal{S}_q^{XY1} + \mathcal{S}_q^{XY2}}{4} \right) + \hbar \left( \frac{\varpi_q^{z+} + \varpi_q^{z-}}{4} \right) \quad (66)$$

<sup>1</sup> Shuzo Kawarazaki et al., Phys. Rev. B **61**, 4167 (2000).

<sup>2</sup> See e.g.: “Magnetism in Heavy Fermion Systems”, Series in Modern Cond. Matter Physics” Vol. 11, Ed. H.B. Radousky, World Sci. (2000); and in particular, Chapter 4: “Neutron Scattering from Heavy Fermions” by R.A. Robinson (p. 197-282), and refs. cited therein.

<sup>3</sup> F. Steglich, J. Aarts, C.D. Bredl, W.Leike, D.E.M.W. Franz, and H. Schäfer, Phys. Rev. Lett. **43**, 1892 (1976); M. Sgrist and K. Ueda, Rev. Mod. Phys. **63**, 239 (1991).

<sup>4</sup> N.D. Mathur, F.M. Grosche, S.R. Julian, I.R. Walker, D.M. Freye, R.K.W. Haselwimmer, and G.G. Lonzarich, Nature **394**, 39 (1998).

<sup>5</sup> M.T.B. Monod et al., Phys. Rev. B **34**, 7716 (1986); D.J. Scalapino et al., Phys. Rev. B **34**, 8190 (1986); G. Aeppli et al., Phys. Rev. Lett. **58**, 808 (1987); N.K. Sato et al, Nature **410**, 340 (2001).

<sup>6</sup> See e.g.: G.R. Stewart, “Non-Fermi-liquid behavior in  $d$ - and  $f$ -electron metals”, Rev. Mod. Phys. Vol. 73, 797-855

(2001); *Addendum* in Rev. Mod. Phys. Vol. 78, 743-753 (2006); and refs. cited therein.

<sup>7</sup> A. Schröder, G. Aeppli, R. Coldea, M. Adams, O. Stockert, H. v. Löhneysen, E. Bucher, R. Ramazashvili, and P. Coleman, Nature **407**, 351 (2000).

<sup>8</sup> R. Küchler, P.Gegenwart, J. Custers, O.Stockert, N. Caroca-Canales, C. Geibel, J.G. Sereni, and F. Steglich, Phys. Rev. Lett. **96**, 256403 (2006).

<sup>9</sup> See e.g. theor. and exp. overview from Kavli I.T.P. Workshop on “Quantum Phase Transitions”(2005), at: <http://online.kitp.ucsb.edu/online/qpt05/>.

<sup>10</sup> B. Coqblin, M.D. Nuñez Regueiro, A. Theumann, J.R. Iglesias, and S. Magalhaes, Phil. Mag. **86**, 2567 (2006).

<sup>11</sup> P. Coleman, review article: “Heavy fermions: electrons at the edge of magnetism”, in Handbook of Magnetism and Advanced Magentic Materials, Vol.1, ed. by H. Krönmüller and S.Parkin, to be published by John Wiley and Sons, Ltd.

- <sup>12</sup> J. Kondo, Progr. Theor. Phys. (Kyoto) **32**, 37 (1964).
- <sup>13</sup> S. Doniach, Proc. "Int. Conf. on Valence Instabilities and Related Narrow-band Phenomena", ed. R.D. Parks, Plenum Press, 168 (1976); Physica **91**, 231 (1977).
- <sup>14</sup> W.P. Beyermann et al, Phys. Rev. B **43**, 13130 (1991).
- <sup>15</sup> A. Severing, E. Holland-Moritz and B. Frick, Phys. Rev. B **39**, 4164 (1989).
- <sup>16</sup> J.R. Iglesias, C. Lacroix and B. Coqblin, Phys. Rev. B **56**, 11820 (1997).
- <sup>17</sup> A.R. Ruppenthal, J.R. Iglesias and M.A. Gusmão, Phys. Rev. B **60**, 7321 (1999).
- <sup>18</sup> B. Coqblin et al., Phys. Rev. B **67**, 64417 (2003).
- <sup>19</sup> J. Rech, P. Coleman, G. Zarand and O.Parcollet, Phys. Rev. Lett. **96**, 16601 (2006).
- <sup>20</sup> N. H. Van Dijk, B. Fak, T. Charvolin, P. Lejay and J.M. Mignot, Phys. Rev. B **61**, 8922 (2000).
- <sup>21</sup> W. Knafo, S. Raymond, B. Fak, G. Lapertot, P.C. Canfield, and J. Flouquet, J. Phys.: Condens. Matter **15**, 3741 (2003).
- <sup>22</sup> V. Vildosola, A.M. Llois, and J.G. Sereni, Phys. Rev. B **69**, 125116 (2004).
- <sup>23</sup> J. Spalek, A. Datta and J. M. Honig, Phys. Rev. Lett. **59**, 728 (1987).
- <sup>24</sup> M. Wagner: "Unitary Transformations in Solid State Physics" (North Holland, Amsterdam 1986), and refs. therein; M.Acquarone and C.I. Ventura, accepted for public. by Int. J. Mod. Phys. B (2006).
- <sup>25</sup> C.I. Ventura and M. Acquarone, Phys. Rev. B **70**, 184409 (2004).
- <sup>26</sup> A.M. Lobos, A.A.Aligia and J.G. Sereni, Eur. Phys. J. B **41**, 289 (2004).
- <sup>27</sup> R. Peters and T. Pruschke, cond-mat/0707.0277 preprint.
- <sup>28</sup> L. Macot and B. Frank, Phys. Rev. B **41**, 4469 (1990).
- <sup>29</sup> D. Golosov, Phys. Rev. B **71**, 14428 (2005).
- <sup>30</sup> F.Ye, P. Dai, J.A. Fernandez-Baca, H. Sha, J.W. Lynn, H. Kawano-Furukawa, Y. Tomioka, Y. Tokura and J. Zhang, Phys. Rev. Lett. **96**, 47204 (2006); F. Ye et al., cond-mat/0702504.
- <sup>31</sup> M.D. Kapetanakis and I.E. Perakis, Phys. Rev. B **75**, (RC) 140401 (2007).

TABLE I: Conduction band AF spin polarization  $\langle s \rangle$  dependence on model parameters, for the cases depicted in respective Figs. 3, 4 and 5. In first column we enter the relative Kondo coupling magnitude (cases of Fig. 3: notice that  $J_K/W \sim J_K/J_H \times 10^{-4}$ , here), while in second column is the corresponding band polarization  $\langle s \rangle$  obtained. Similarly in third column we enter the electron correlation  $U/W$  cases from Fig. 4, and next the corresponding  $\langle s \rangle$ . In 5th column we enter filling  $n$  values of Fig. 5, and in last column the corresponding  $\langle s \rangle$  values.

$J_K/J_H$	$\langle s \rangle$	$U/W$	$\langle s \rangle$	$n$	$\langle s \rangle$
0.1	0.2152	0.008	0.0002	0.999	0.2153
1.	0.2153	0.08	0.001	0.8	0.1675
5.	0.2157	0.25	0.215	0.7	0.1329
10.	0.2163	0.5	0.406	0.6	0.0796
15.	0.2168	0.83	0.480	0.4	0.00006